J. Geotech, Eng., JSCE, No. 708/III-59, 1-11, 2002 June

PERMEABILITY ANISOTROPY OF SHIRAHAMA SANDSTONE UNDER TRUE TRIAXIAL STRESSES

Xiaochun LI[1], Zhishen WU[2], Manabu TAKAHASHI[3] and Kazuya YASUHARA[4]

[1] Dr. Eng., Dept. of Urban & Civil Eng., Ibaraki University
(4-12-1 Nakanaruzawa, Hitachi, Ibaraki 316-8511, Japan)
E-mail:xli@rite.or.jp

[2, 4] Member of JSCE, Dr. Eng., Professor, Dept. of Urban & Civil Eng., Ibaraki University
(4-12-1 Nakanaruzawa, Hitachi, Ibaraki 316-8511, Japan)

[3] Member of JSCE, Dr. Eng., Research Center for Deep Geological Environments, AIST
(1-1-3 Higashi, Tsukuba, Ibaraki 305-8567, Japan)

Anisotropic stresses may induce anisotropic permeability of rocks. The present study aims at establishing the relation between permeability tensor and principal stresses for Shirahama sandstone within the pre-yield range. The effects of three principal stresses on the permeability are experimentally investigated using a Mogi-type true triaxial apparatus and transient pulse technique. Stress sensitivity coefficients of permeability are defined to describe the influence coefficients of stresses, which are found to be independent of stress states and loading paths. Based on these observations, we proposed a linear relation between the logarithm of the principal components of permeability tensor and the principal stresses.

Key Words: *permeability, anisotropy, true triaxial stress, Shirahama sandstone*

1. INTRODUCTION

The study on the physics of flow and transport through porous rocks is of fundamental importance to many applied scientific and engineering fields related to underground fluid flow. Rock permeability is, without doubt, a key parameter in any model of fluid flow and transport through rocks. Early models assumed uniform and invariant permeability values for each stratum[1)-3)]. In these studies, permeability is regarded as an independent and isotropic parameter of the rocks. It is well known that the permeability is determined by the pore structure of the rock, and therefore, any process that results in the change of pore structure may affect the permeability.

A macroscopic stress field alters the arrangement and shape of particles and pores. Therefore, the permeability change of rock materials usually occurs. Permeability reduction in rocks under hydrostatic pressures has been extensively studied by many researchers for a wide range of rock materials, from porous sediments to dense, crystalline, igneous rocks[4)-8)]. Moreover, the influence of axial stress on fluid transport properties has also been investigated for a limited number of rock types[9)-12)].

Recently, a few studies have been carried out on the influence of true triaxial stresses on the fluid transport properties[13)-17)]. The experimental observations on the permeability changes induced by anisotropic stresses serve as basis for constructing the stress-permeability relationship that is necessary to model mechanical-hydraulic coupling behavior of rocks. Skoczylas and Henry[15)] investigated the permeability change of 50cm-cubic intact and fractured granite blocks with a 30mm-diameter central hole under three principal stresses: one in the direction parallel to the hole axis and the others, perpendicular. The permeability in the radial direction of the hole was measured by transient pulse technique

using argon or neon as permeating media. It is realized that the lateral permeability reduction was associated mainly with increase of the stresses perpendicular to the hole axis, which was explained by assuming existence of radial microcracks. In experimental arrangement mentioned above, because the two stresses perpendicular to the hole axis were equal to each other, their separate effects can not be explicitly recognized. In the work by King *et al.*[16), 17)], cubic specimens of initially isotropic sandstones were cracked by a differential stress applied by three pairs of rigid platens, and then, the effect of the stress perpendicular to the plane of the cracks on the permeability was investigated. They argued that there was a relationship between the changes in the ultrasonic velocities and permeability induced by the stresses. The above studies highlight the role of aligned discontinuities and the normal stress in dominating transport property. However, the effect of the stresses in other directions is not clear yet. Takahashi *et al.*[13) 14)], using the transient pulse technique, investigated the effects of three stresses on permeability in the direction of the maximum principal stress for Shirahama sandstone. Their experimental results showed that the effect of the maximum principal stress is more significant than that of the intermediate principal stress. The question is whether this conclusion can be reached if the fluid flows in the direction of the intermediate or minimum principal stresses.

The present study aimed at establishing a general relationship between three principal components of permeability tensor k_i (i =1, 2, 3) and three principal stresses σ_i (i=1, 2, 3) within the pre-yield range for Shirahama sandstone. For this purpose, stress sensitivity coefficients of permeability were defined to quantitatively describe the affecting extent of the stresses. An experimental technique has been developed where transient pulse permeability measurement technique has been incorporated into a Mogi-type true triaxial apparatus[18)]. Using the technique, experiments have been conducted to investigate the effects of stress states and loading path on the permeability. Finally, based on the experimental results, a simple stress-permeability relation has been proposed.

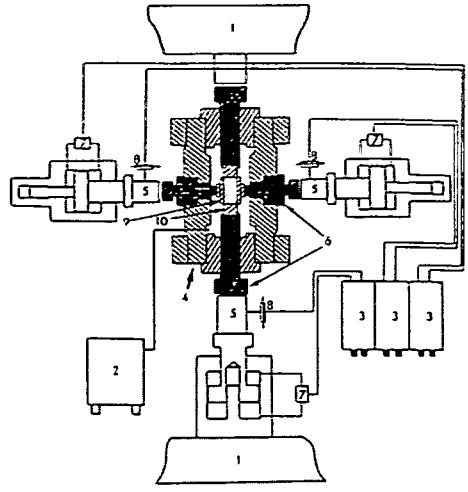

Fig.1 Schematic diagram of the true triaxial apparatus. 1-Upper and lower platens, 2-Hydraulic power supply, 3-Controll unit, 4-Pressure vessel, 5-Load cells, 6-Pistons, 7-Servo valves, 8-LVDTs, 9, 10-End pieces.

2. EXPERIMENTAL TECHNIQUES

(1) Test equipments

The tests were conducted using the true triaxial apparatus of Geological Survey of Japan[19)]. This Mogi-type, servo-controlled apparatus enables three principal compressive stresses to be applied independently (**Fig.1**). One of the characteristics of this loading apparatus is that it exerts two principal stresses by rigid pistons and the other stress directly by oil pressure. **Fig.2** schematically shows the experimental arrangement. The Shirahama sandstone rectangular parallelepiped specimens were placed in the center of the true triaxial apparatus. We define the stress in the vertical direction as σ_1, one of the lateral stresses exerted by the pistons as σ_2, and the stress, directly by oil pressure, as σ_3. Note that σ_1, σ_2 and σ_3 are not necessarily maximum, intermediate and minimum principal stresses, respectively. Also, the permeabilities in the directions of σ_1, σ_2 and σ_3 are denoted as k_1, k_2 and k_3, respectively. As shown in **Fig.2**, the specimen (1) was jacketed with silicon rubber (5). 0.05mm thick Teflon sheet and copper foil were placed between the specimen (1) and end pieces (2, 3) to eliminate the frictions and interfacial flows.

In the σ_2–direction, the specimen (1) was connected to permeability measurement apparatus with a capacity of 40MPa pore pressure, via porous metals (4), end pieces (2) and pipes (11). Each porous metal (4) with 66 holes (1mm in diameter) was

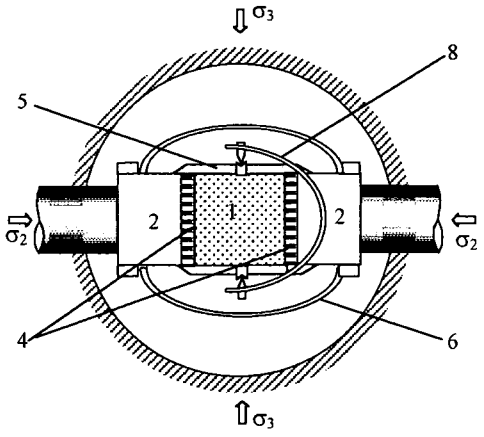

View from σ_1

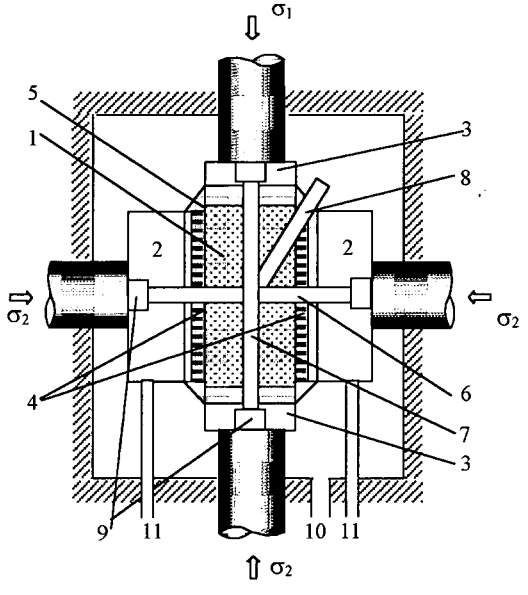

View from σ_3

Fig.2 Schematic diagram of specimen assembly. 1-Specimen, 2, 3-End pieces, 4-Porous metals, 5-Silicon rubber, 6, 7, 8-Displacement transformers for σ_2, σ_1, σ_3-direction respectively, 9-Stopper for displacement transformer, 10-Oil inlet, 11-Pore water inlet

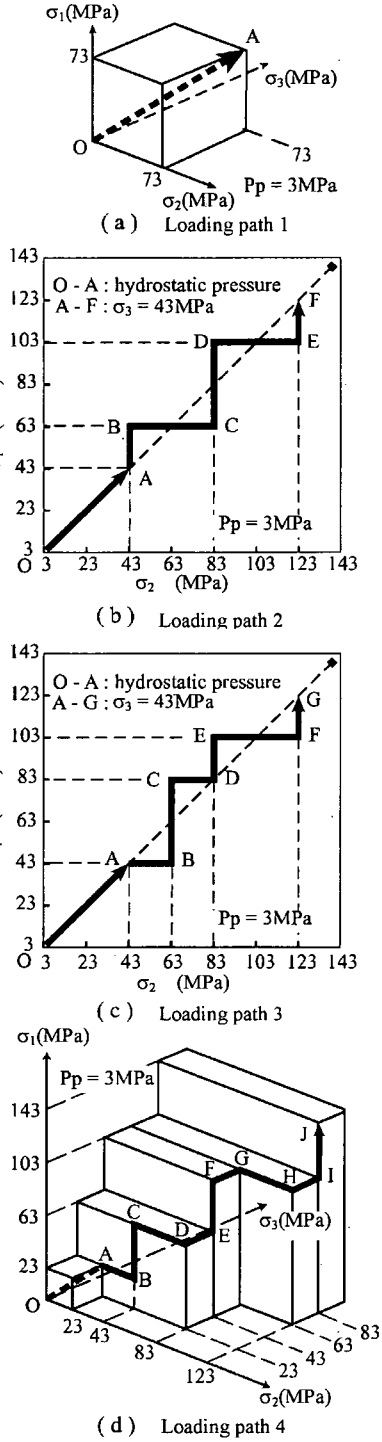

Fig.3 Loading paths

designed here to distribute the pore water to the surface of the specimen. The permeability was measured with a transient pulse technique, originated by Brace *et al*[4]. After the pore pressure equilibrated in the specimen, the fluid pressure was raised instantaneously by 0.05MPa at one end of the specimen. The fluid pressure at this end then decreased, while the fluid pressure at the other end increased with time as the fluid flowed through the specimen, i.e. the differential pressure decayed with time. The permeability can be calculated according to the speed of the differential pressure decay. This sophisticated technique has been used in the laboratory of Geological Survey of Japan for a decade[20].

The deformations in three directions were measured using five cantilever-type displacement transformers (6, 7, 8) with a sensitivity of 15-30με, on which four strain gages were mounted in full bridge configuration.

(2) Some aspects of the experimental technique

A few important improvements have been made in the experimental arrangements.

In our arrangement, the specimen was placed in the pressure vessel of the Mogi-type loading apparatus (**Fig.2**), i.e., in a confining pressure ambience, unlike the arrangements of Skoczylas and Henry.[15] and King *et al.*[16), 17] where the specimen was in atmospheric ambience. The pore pressure should be lower than the ambient pressure to prevent the jacket material from bulging, even from fracturing. Thus, the present arrangement allows a higher pore pressure up to 100MPa.

Our arrangement is similar to that of Takahashi *et al.*[13), 14], but with some important improvements. One of the improvements is that the permeability in σ_2-direction was measured [13), 14]. Usually, in the true triaxial tests, σ_1 is the maximum principal stress and σ_2 is the intermediate principal stress. It is well known that the eventual fault is parallel to the intermediate principal stress direction, i.e., σ_2–direction, but with a slant angle with respect to the maximum principal stress, i.e. σ_1-direction. Such an improvement made the measurements of transport properties of faults formed under various stress states possible. Another advantage is that the time needed for permeability measurement was considerably shortened. The time-consumption is directly proportional to the length of flow path and inversely proportional to the cross area. Because the length of the flow path and the cross area in our arrangement were 1/2 and 2 times of those by Takahashi *et al.*[13) 14], respectively, for a specimen of same size, the time consumption was 1/4 of that by Takahashi *et al.*[13), 14].

(3) Specimen description

The specimen was a rectangular parallelepiped with dimensions of 70×34×34mm. It was prepared with its longer sides perpendicular to the bedding planes.

The petrographical properties of Shirahama sandstone have been investigated in the previous study[21]. This rock mainly consists of quartz grains and rock fragments, with an average grain size of 0.15mm and a porosity of 11%. Prior to the tests, the P-wave velocities in three directions of 51 specimens have been measured to investigate the anisotropic property. The average P-wave velocities in 1-, 2-, and 3-direction were 2.74, 2.89 and 2.89km/s, respectively, exhibiting transverse isotropy, like most of bedded sedimentary rocks.

Table 1 Yield stress under different stress conditions

σ_3 (MPa)	23.0	43.0	63.0	83.0
σ_2 (MPa)	63.0	83.0	103.0	123.0
Yield stress (MPa)	91.6	127.0	151.1	175.9

Note: The pore pressure was 3MPa for all the cases.

(4) Test procedures

This study concentrated on investigating the effect of three principal stresses and loading paths on the permeability in σ_2-direction, k_2, within the pre-yield range. For this purpose, fore kinds of loading paths were designed, wherever the pore pressure, p_p, was kept constant at 3MPa.

In loading path 1 (specimen No.ss-22), hydrostatic pressure, p_c was applied up to 73MPa to investigate the combined effects of three principal stresses (**Fig.3(a)**).

In loading path 2 (specimen No.ss-21), first, the hydrostatic pressure was applied to 43MPa. Second, σ_1 and σ_2 were increased alternately while σ_3 was kept constant at 43MPa (**Fig.3(b)**).

The loading path 3 is similar to the loading path 2, but different in the loading order of σ_1 and σ_2 (**Fig.3(c)**).

In loading path 4 (specimen No.ss-27), first, hydrostatic pressure was applied to 23MPa (0-A), and then, σ_2, σ_1 and σ_3 were increased alternately (A-J). In this process, any one of three principal stresses was increased while the other two stresses were kept constant (**Fig.3(d)**).

During the above loading processes, cares were taken to avoid the specimen yielding. The failure strength, i.e., maximum principal stress at failure, under different minimum and intermediate principal stresses was measured. 60% of the failure strength was taken as the yield stress (**Table 1**). In the four loading paths, the maximum principal stress was never higher than the corresponding yield stress to avoid yielding.

3. EXPERIMENTAL RESULTS

(1) Effect of hydrostatic pressure

The effect of the hydrostatic pressure on permeability is shown in **Fig.4**, where k^a_2 is the permeability at p_c=2MPa, and p_c is effective hydrostatic pressure defined as the hydrostatic pressure minus the pore pressure. This figure is made based on the experimental results of step O-A of the loading path 1-4 (**Fig.3**). Reduction in permeability with the increase of p_c is apparent. The permeability decreases in a similar manner for 4 specimens. The rate of change of the permeability with the increasing effective hydrostatic pressure is greater at low effective hydrostatic pressure less than about 15MPa. Similar results for Shirahama sandstone were also reported by Takahashi *et al.*[13] and Lin *et al*[22]. Takahashi *et al.*[13] observed the closures of preexisting pores in a specimen that had experienced a hydrostatic compression of 49MPa. Thus, the rapid reduction at low hydrostatic pressure may be interpreted in terms of the closures of the pores with low aspect ratios. Over this loading level, it seems that $\log_{10}(k_2/k^a_2)$ can be regarded as a linear function of p_c. Pressure sensitivity coefficient of permeability, α_{2p} is defined as equation (1), the absolute value of which represents the extent to which the effective hydrostatic pressure p_c affects the permeability in σ_2-direction.

$$\alpha_{2p} = d(\log_{10} k_2)/dp_c \qquad (1)$$

where α_{2p} is in MPa^{-1} and p_c, in MPa. The pressure dependent permeability in the linear range, i.e. $p_c \geq 15$MPa, can be expressed as:

$$\log_{10}(k_2/k^0_2) = \alpha_{2p} p_c \qquad (2)$$

where k^0_2 is an apparent initial permeability, corresponding to the value of k_2 at p_c=0 on the regression line. α_{2p} can be obtained by mean square linear regression over the linear range of the curve in **Fig.4**. Based on the experimental results the value of α_{2p} is identified as -5.82×10^{-3}/MPa (**Fig.4**). k^0_2 can be calculated as 1.98×10^{-5}darcy, for example, by substituting the average value of the permeability of 1.47×10^{-5}darcy measured under a effective hydrostatic pressure of 20MPa into equation(2).

(2) Effects of the principal stresses

Hereinafter, we'll deal with the effects of the three principal stresses on the permeability.

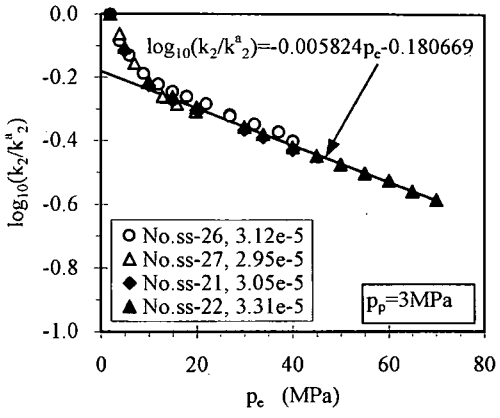

Fig.4 $\log_{10}(k_2/k^a_2)$ as a function of effective hydrostatic pressure, $p_e(=p_c-p_p)$. k^a_2 is the value of permeability in darcy, indicated in the legend at a hydrostatic pressure p_c of 5MPa and pore pressure p_p of 3MPa. The equation is obtained by mean square linear regression for all the specimens under p_e>15MPa.

Assuming loading path independence during monotonic loading within the pre-yield range, permeability tensor k_{ij} can be expressed as a function of effective stress tensor σ'_{kl}.

$$\log_{10} k_{ij} = f_{ij}(\sigma'_{kl}) \qquad (i, j = x, y, z) \qquad (3)$$

This assumption need be confirmed by experiments, which is why the four loading paths were designed. An increment in stresses will cause a variation in permeability as

$$d\log_{10} k_{ij} = \frac{\partial f_{ij}}{\partial \sigma'_{kl}} d\sigma'_{kl} \qquad (4)$$

To obtain the form of the functions f_{ij} and quantitatively interpret the experimental results, we define stress sensitivity coefficients of permeability α_{ijkl} that describe the extent to which a stress component affects a permeability component.

$$\alpha_{ijkl} = \partial f_{ij} / \partial \sigma'_{kl} \qquad (5)$$

Because there are 6 independent components in both the permeability tensor and effective stress tensor, respectively, α_{ijkl} have 36 independent components. At present, it is unrealistic to measure all of them, especially those involved in shear stresses. To make the problem traceable, we concentrated on a special case where the principal axes of the permeability tensor coincide with those of the stress tensor. This is just the case of our experimental arrangements. In such a way, only those components of α_{ijkl}

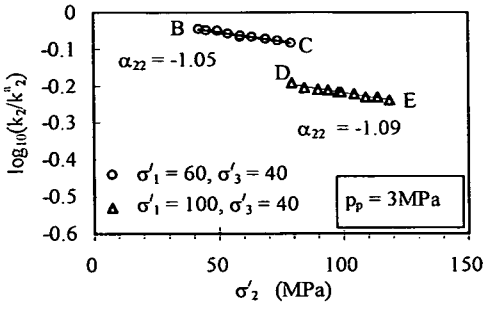

(a) Loading path 2 (No. ss21, k^a_2 = 1.14e-5darcy)

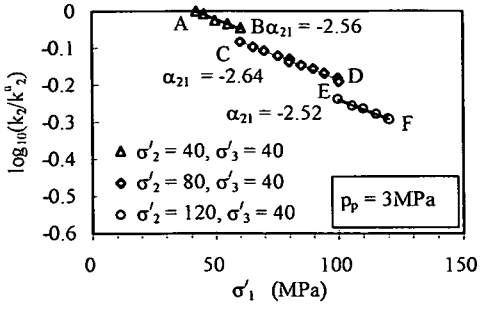

(a) Loading path 2 (No. ss21, k^a_2 = 1.14e-5darcy)

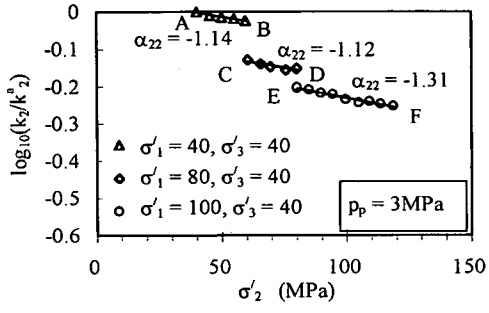

(b) Loading path 3 (No.ss26, k^a_2 =1.23e-5darcy)

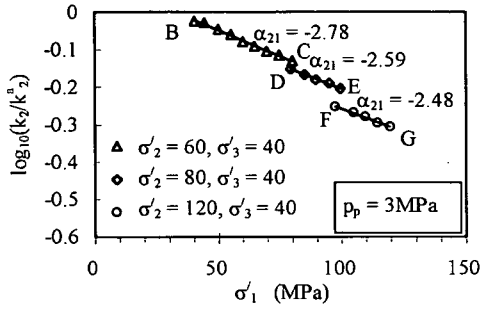

(b) Loading path 3 (No.ss26, k^a_2 =1.23e-5darcy)

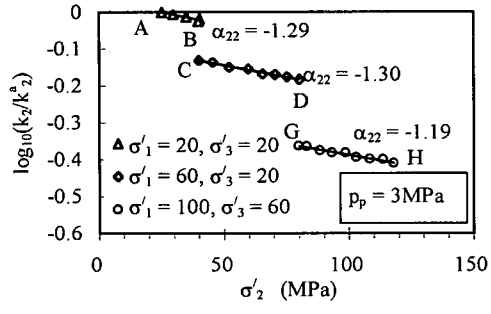

(c) Loading path 4 (No.ss27, k^a_2 =1.46e-5darcy)

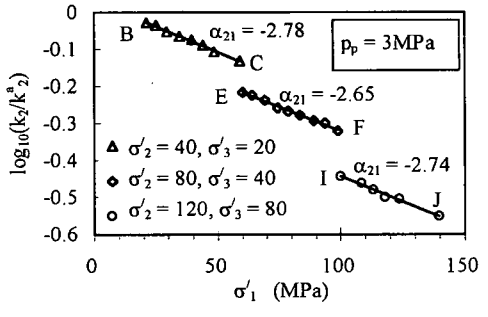

(c) Loading path 4 (No.ss27, k^a_2 =1.46e-5darcy)

Fig.5 $\log_{10}(k_2/k^a_2)$ as a function of σ'_2 under various stress conditions indicated in the legends and boxes in MPa. The values of k^a_2 are given in the sub-captions (see text). The values of α_{22} are obtained by mean square linear regression over the corresponding loading steps, in 10^{-3}MPa^{-1}.

Fig.6 $\log_{10}(k_2/k^a_2)$ as a function of σ'_1 under various stress conditions indicated in the legends and boxes in MPa. The values of k^a_2 are given in the sub-captions (see text). The values of α_{21} are obtained by mean square linear regression over the corresponding loading steps, in 10^{-3}MPa^{-1}.

with i=j and k=l still exist in equation(4). For the sake of simplicity, we rewrite equation (4) and (5) as

$$d\log_{10} k_i = \alpha_{ij} d\sigma'_j \qquad (i, j = 1, 2, 3) \quad (6)$$

$$\alpha_{ij} = \partial \log_{10} k_i / \partial \sigma'_j \qquad (i, j = 1, 2, 3) \quad (7)$$

where the subscripts 1, 2, 3 denote principal stress or principal permeability to avoid misunderstanding.

Stress sensitivity coefficients of permeability α_{ij} are crucial parameters relating permeability to stresses. The experiments were conducted to measure their values and examine their dependency on loading paths and stress states within pre-yield range.

Fig.5, **Fig.6** and **Fig.7** show the effects of the effective principal stresses on the permeability in

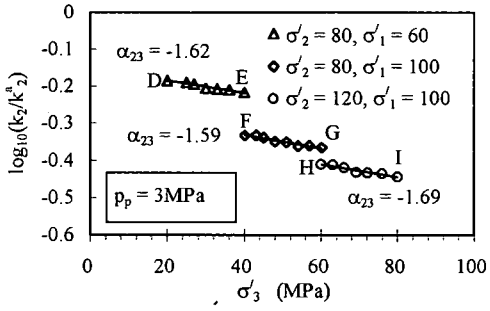

Loading path 4 (No.ss27, k^a_2 =1.46e-5darcy)

Fig.7 $\log_{10}(k_2/k^a_2)$ as a function of σ'_3 under various stress conditions indicated in the legends and boxes in MPa. The values of k^a_2 are given in the sub-captions (see text). The values of α_{23} are obtained by mean square linear regression over the corresponding loading steps, in 10^{-3}MPa^{-1}.

σ_2-direction, where $\log_{10}(k_2/k^a_2)$ is plotted as a function of σ'_1, σ'_2 and σ'_3, respectively. **Fig.5(a)** is made based on the experimental results from the step B-C and step D-E of the loading path 2 (**Fig.3(b)**), **Fig.5(b)**, the step A-B, step C-D and step E-F of the loading path 3 (**Fig.3(c)**) and **Fig.5(c)**, the step A-B, step C-D and step G-H of the loading path 4 (**Fig.3(d)**). k^a_2 is the permeability at $\sigma'_1 = \sigma'_2 = \sigma'_3$ = 40MPa for loading path 2 (**Fig.5(a)**) and loading path 3 (**Fig,5(b)**), and at $\sigma'_1 = \sigma'_2 = \sigma'_3$ = 20MPa for loading path 4 (**Fig,5(c)**). **Fig.6** and **Fig.7** are made in the same way. As shown in **Fig.5-Fig.7**, increasing of the principal stresses in any directions results in reduction of the permeability. The data **in Fig.5-Fig.7** indicate the values of α_{ij} of each loading step, obtained by mean square linear regression.

4. DISCCUSSIONS

Hereinafter, we will discuss the effects of stress states and loading paths, and accordingly establish a relationship between permeability and stresses.

(1) Effect of stresses in terms of maximum, intermediate and minimum principal stresses

Takahashi *et al.*[13), 14)] have discussed the effects of stresses on the permeability in terms of the maximum, intermediate and minimum principal stresses. They argued the effect of the maximum principal stress is more significant than that of the intermediate principal stress. However, noting step B-C and D-E in **Fig.5(a)**, step E-F in **Fig.5(b)** and step C-D

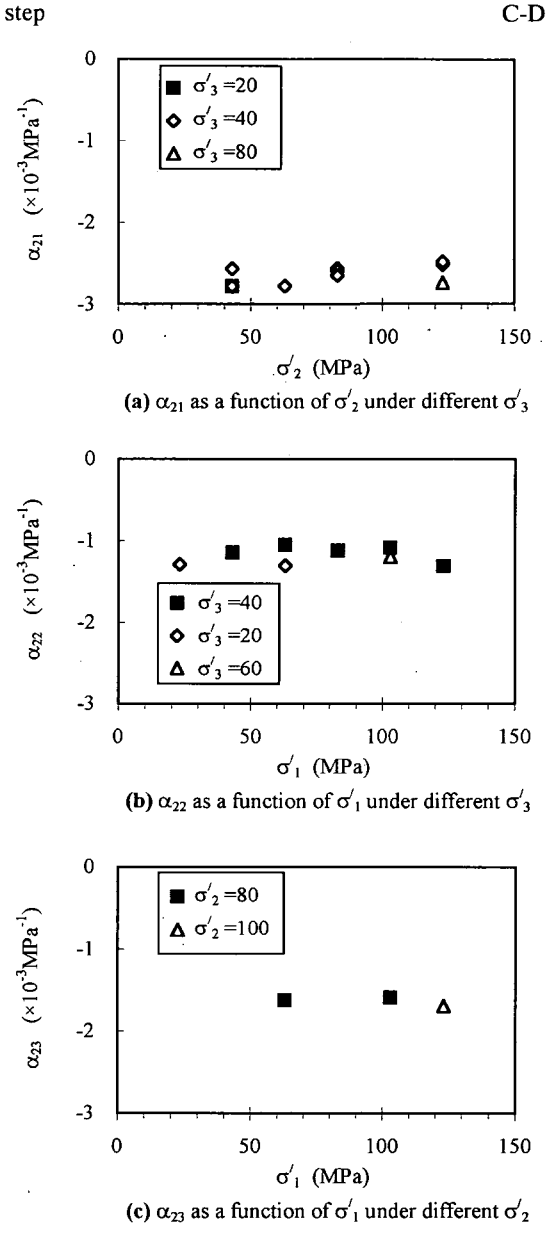

(a) α_{21} as a function of σ'_2 under different σ'_3

(b) α_{22} as a function of σ'_1 under different σ'_3

(c) α_{23} as a function of σ'_1 under different σ'_2

Fig.8 Stress sensitivity coefficients of permeability as a function of the effective principapal stresses. The stress data in the boxes are in MPa

and G-H in **Fig.5(c)**, where σ_2 increases from intermediate principal stress to maximum principal stress (**Fig.3**), the slopes of the curves do not change remarkably. The same argument can be drawn from the observations of step C-D in **Fig.6(a)**, step B-C in **Fig.6(b)** and step B-C, E-F and I-J in **Fig. 6(c)**, where σ_1 changes from intermediate principal stress to maximum principal stress (**Fig.3**). These observa-

Table 2 Pressure and stress sensitivity coefficients of permeability under various stresses and loading paths.

Stresses (MPa)			Loading paths	α_{ij}($\times 10^{-3}$MPa^{-1})			
σ_2	σ_1	σ_3		α_{22}	α_{21}	α_{23}	α_{2p}
15-43	15-43	15-43	1				-5.93
15-43	15-43	15-43	1				-5.80
15-73	15-73	15-73	1				-5.73
							-5.82*
43-83	63	43	2	-1.05			
83-123	103	43	2	-1.09			
43-63	43	43	3	-1.14			
63-83	83	43	3	-1.12			
83-123	123	43	3	-1.31			
23-43	23	23	4	-1.29			
43-83	63	23	4	-1.30			
83-123	103	63	4	-1.19			
				-1.19*			
43	43-63	43	2		-2.56		
83	63-103	43	2		-2.64		
123	103-123	43	2		-2.52		
63	43-83	43	3		-2.78		
83	83-103	43	3		-2.59		
123	103-123	43	3		-2.48		
43	23-63	23	4		-2.78		
83	63-103	43	4		-2.65		
123	103-143	83	4		-2.74		
					-2.63*		
83	63	23-43	4			-1.62	
83	103	43-63	4			-1.59	
103	123	63-83				-1.69	
						-1.63*	

Note: *the average of α_{2p} , α_{22} , α_{21} or α_{23}, respectively.

tions suggest that values of α_{ij} are not associated with whether the stresses are maximum, intermediate or minimum principal stress. Thus, there is no need to distinguish which is the maximum, intermediate or minimum principal stress in equation (6).

(2) Effects of the stress states and loading paths on k_2

The values of α_{ij} under different loading paths and stress conditions **(Fig.5-Fig.7)** are summarized as shown in **Table 2** and illustrated in **Fig.8**. **Fig.8(a)** demonstrates the effect of σ'_1 on α_{22} under different σ'_3. The fact that the values of α_{22} measured under various levels and loading paths do not show significant variations suggests that it can be approximately considered to be independent of loading paths and stress states. Also, the same arguments can be made for α_{21} and α_{23} **(Table 1, Fig.8(b)** and **Fig.8(c))**.

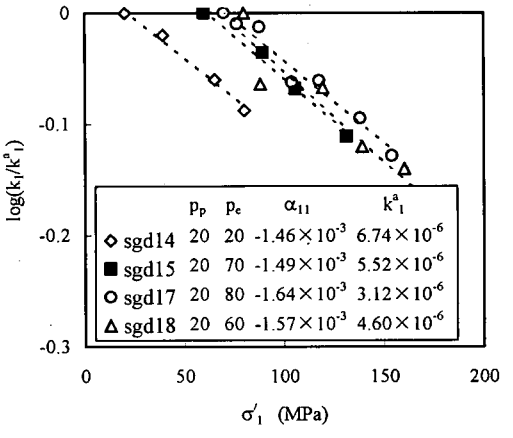

Fig.9 $\log_{10}(k_1/k^a_1)$ as a function of the effective axial stress σ'_1 under different effective confining pressures p_e. The pore pressure p_p and effective confining pressure p_e are in MPa. The values of α_{11} (in MPa^{-1}) are obtained by mean square linear regression. k^a_1, in darcy, is the permeability at the corresponding p_e with differential axial stress=0.

(3) Effects of stress states paths on k_1

We have not measured the permeability in σ_1 and σ_3-direction in this study. However, due to the transverse isotropy of Shirahama sandstone, α_{31}, α_{32} and α_{33} can also be considered as constants. The characteristics of α_{11}, α_{12} and α_{13}, which reflect the effects of stresses on the permeability perpendicular to the bedding planes may be inferred from the pre-

vious studies.

First we address the effect of hydrostatic pressure. Lin *et al.*[22] have measured the permeability perpendicular to the bedding planes, k_1, for Shirahama sandstone under hydrostatic pressures, using a conventional triaxial apparatus and transient pulse technique. They plotted the results together with those reported by Takahashi *et al.*[8), 14)]. The results of the 6 specimens reported by Takahashi *et al.* showed a considerable variance in the values of the permeability. Nevertheless, it seems that a linear relation between the $\log_{10}k_1$ and p_e can be recognized when p_e is not less than some lower limit of around 10MPa for most of the specimens except No.T1991 (SS-7) and No.T1993. For the specimen No.T1993[14)], the lower limit seems to be about 30MPa. Lin *et al.*'s results showed a fairly good linearity and repeatability. Therefore, α_{1p}, defined similarly as equation (2), can be regarded as constant.

Second, we address the effect of σ_1. Li *et al.*[12] have investigated axial stress-induced change in the permeability under different confining pressure for Shirahama sandstone, where both the axial stress and the flow is perpendicular to the bedding planes. The results are replotted here in the semi-logarithm coordinates (**Fig.9**). The figure shows that α_{11} varies in a narrow range from 1.46 to 1.64×10^{-3} MPa^{-1} under different effective confining pressure.

Moreover, Takahashi *et al.*[14)] have measured the effects of the maximum and intermediate principal stresses, corresponding to σ_1 and σ_2, respectively, on k_1. It seems that the extents to which the effects of both σ_1 and σ_2 are greater than those of the present study, and depend on the stress states. This possibly arose from that the minimum principal stress (15MPa) exerted was smaller than the lower limit of 30MPa above mentioned.

Therefore, assuming α_{ij} to be constant within some stress range does not conflict with the existing experimental results for Shirahama sandstone.

(4) Relationship between permeability and stresses

Because stress sensitivity coefficients of permeability α_{ij} can be regarded independent of stress states and loading paths, integration of equation (4) can deduce

$$\log_{10}(k_i / k_i^0) = \alpha_{ij}\sigma'_j \qquad (i, j = 1, 2, 3) \quad (8)$$

where k_{i0} is the apparent initial value of permeability, not real initial value.

Equation(8) is valid on such conditions as:

a) Any one of the principal stresses must be increased monotonically, without loading-unloading cycles. Many researchers[23), 24)] have reported that permeability of rocks, including Shirahama sandstone[22)], generally exhibits hysteresis during hydrostatic pressure loading-unloading cycles. It may also do so during complex stress cycles.

b) The stress states must be within such a range as not beyond yield limit and not less than some lower effective stress limit of 15MPa for Shirahama sandstone.

Beyond the above conditions, the relation may be nonlinear. These problems are beyond the present study and need further investigations.

Equation(8) has an important implication that the effect of combined stresses is equivalent to summation of that of individual stresses. **Table 1** contains the average values of α_{2p}, α_{21}, α_{22} and α_{23}. It is interesting to note that the sum of the average values of α_{21} , α_{22} and α_{23} is $-5.45\times10^{-3}MPa^{-1}$ which is approximately equal to that of α_{2p} of -5.82×10^{-3} MPa^{-1}.

For anisotropic materials, there exist 9 independent parameters α_{ij} ,and 3 initial values of permeability k_{i0}, in equation(8). For transversely isotropic material such as bedded sedimentary rocks like Shirahama sandstone, if the symmetric axis is in σ_1-direction, the following relations can be deduced.

$$\begin{aligned} \alpha_{21} &= \alpha_{31} \\ \alpha_{22} &= \alpha_{33} \\ \alpha_{23} &= \alpha_{32} \\ \alpha_{13} &= \alpha_{12} \\ k_2^0 &= k_3^0 \end{aligned} \qquad (9)$$

Thus, in case of transverse isotropy, only 5 out of 9 components of α_{ij} , and 2 out of 3 initial values of permeability k^0_i, 7 components in all, are independent. From the present experimental results, 4 components can be obtained as

$$\begin{aligned} \alpha_{21} &= -2.63\times10^{-3}MPa^{-1} \\ \alpha_{22} &= -1.19\times10^{-3}MPa^{-1} \\ \alpha_{23} &= -1.63\times10^{-3}MPa^{-1} \\ k_2^0 &= 1.98\times10^{-5}darcy \end{aligned} \qquad (10)$$

The other three components may be determined by conducting permeability measurements in the σ_1-direction.

As shown in equation(10), the value of α_{21} is greater than that of α_{23} and α_{22}. Note that, in our experiments, the stress σ_1 was perpendicular to the bedding planes. This indicates that the permeability is most sensitive to the stress perpendicular to the bedding plane, which agrees with the results of Takahashi *et al.*[13) 14)].

5. CONCLUSSIONS

Stress sensitivity coefficients of permeability was defined to describe the effects of true triaxial stresses, with which stress-permeability relations are formulated. An experimental technique is developed by incorporating transient pulse technique into Mogi-type true triaxial apparatus, which allow a high pore pressure to be applied and enable a permeability measurement in the full process from elastic deformation to eventual faulting. Using this technique, we have investigated the effects of three principal stresses and loading paths on permeability of Shirahama sandstone. According to the experimental results, some of independent components of stress sensitivity coefficients of permeability are obtained. Through these experimental investigations and modeling, the following conclusions may be reached: 1). The components of stress sensitivity coefficients of permeability are different from each other. 2). Stress sensitivity coefficients of permeability is independent of stress states and loading paths under monotonic loading and within such a range not beyond yield limit and not less than some lower limit. Based on these observations, we propose a linear relation between the principal components of the logarithm of permeability tensor and principal stresses. Permeability is most sensitive to the stress perpendicular to the bedding planes.

REFERENCES

1) Norton, D. L. and Taylor, H. P. Jr.: Quantitative simulation of the hydrothermal system mineralization of crystallizing magmas on the basis of transport theory and oxygen isotrope data: an analysis of the Skaergaard intrusion. *Journal of Petrology*, Vol.20, pp.421-486, 1979.

2) Bickle, M. J. and Mckenzie, D.: The transport of heat and matter by fluid during metamorphism. *Contributions to Mineralogy and Petrology*, Vol.95, pp.385-392, 1987.

3) Baumgartner, L. P. and Rumble, D.: Transport of stable isotopes: ¯Development of a kinetic continuum theory for stable isotope transport. *Contributions to Mineralogy and Petrology*, Vol.98, pp.417-430, 1988.

4) Brace, W. F., Walsh, J. B. and Frangos, W. T.: Permeability of granite under high pressure, *J. Geophys. Res.*, Vol.73, pp.2225-2236, 1968.

5) Brace, W. F.: Permeability of crystalline and argillaceous rocks. *Int. J. Rock Mech. Min. Sci. Geomech. Abstr.*, Vol.17, pp.241-251.

6) Gangi, A. F.: Permeability of unconsolidated sands and porous rocks, *J. Geophys. Res.*, Vol.90(B4), pp.3099-3140, 1982.

7) Zhang, S., Paterson, M. S. and Cox, S. F.: Porosity and permeability evolution during hot isostatic pressing of calcite aggregates. *J. Geophys. Res.*, Vol.99(B8), pp.15741-15760, 1993.

8) Takahashi, M., Xue, Z. and Koide, H.: On the permeability of Inada granite, Shirahama sanstone, Kimashi sandstone and Neogene argillaceous rock, *Belletin of the Geological Survry of Japan*, Vol.42, No.6-7, pp.305-331,1991.

9) Zoback, M. D. and Byerlee, J. D.: The effect of microcrack dilatancy on the permeability of Westerly granite, *J. Geophys. Res.*, Vol.80, pp.752-755, 1975.

10) Brace, W. F.: A note on permeability change in geologic material due to stress, *Pur. Appl. Geophys.*, Vol.116, pp.627-633, 1978.

11) Zhu, W. and Wong T.-f.: The transition from brittle faulting to cataclastic flow: Permeability evolution, *J. Geophys. Res.*, Vol.102(B2), pp.3027-3041, 1997.

12) Li, X., Takahashi, M. and Zhang, M.: Relationship between ductile behavior and permeability for Shirahama sandstone, *Proc. 10th Japan Symposium on Rock Mechanics,* pp.707-712, Tokyo, Japan, 1998.

13) Takahashi, M., Koide, H. and Sugita, Y.: Three principal stress effects on permeability of shirahama sandstone, *Proc. 8th International Congress on Rock Mechanics*, Fujii, T. eds., A. A. Balkema Publishers, Tokyo, Japan, pp.729-732, 1995.

14) Takahashi, M., Sugita, Y and Xue, Z.: Three principal stress effects on permeability of Shirahama sandstone—In case of stress state prior to dilatancy, *J. The Mining and Materials Processing Institute of Japan*, Vol.109, pp.803-808, 1993.

15) Skoczylas, F. and Henry, J. P.: A study of the intrinsic permeability of granite to gas, *Int. J. Rock Mech. Min. Sci. Geomech. Abstr.*, Vol.32, pp.171-179, 1995.

16) King, M. S., Chaudhry, N. A. and Shakeel, A.: Experimental ultrasonic velocities and permeability for sandstone with aligned cracks, *Int. J. Rock Mech. Min. Sci. Geomech.*

Abstr., Vol.32, pp.155-163, 1995.

17) King, M. S., Shakeel, A. and Chaudhry, N. A.: Acoustic wave propagation and permeability in sandstone with systems of aligned cracks, *Developments in Petrophysics*, Geological Society Special Publication No.122, Lovell, M. A. and Harvey, P. K. eds, pp.69-85, 1997.

18) Mogi, K.: Effect of triaxial stress systems on the failure of dolomite and limstome, *Tectonophysics*, Vol.11, pp.111-127, 1971.

19) Takahashi, M., Koide, K. and Kinoshita, S.: Characteristics of strength in sedimentary rocks under true triaxial compressional stress state and the increase of brittleness on the intermediate stress, *J. of The Japan Society of Engineering Geology*, Vol.24, No.4, pp.10-17, 1983.

20) Takahashi, M. and Xue, Z.: On some problems in transient pusle technique for permeability measurements, *Chishitsu News*, No.421, pp.46-54, 1989.

21) Takahashi, M. and Li, X.: Change in Microstructure of Shirahama sandstone during Brittle-Ductile deformation, Proc. Hokkaido Geotechnics'98, pp.27-32, 1998.

22) Lin, W., Takahashi, M., Li, X. and Suzuki, K.: Comparison of the permeability of Shirahama sandstone specimen facketed with different mrthods, *J. Japan Soc. Eng. Geol.*, Vol.40, No.5, pp.299-305, 1999.

23) Sutherland, H. J. and Cave, S. P.: Argon gas permeability of New Mexico rock salt under hydrostatic compression, *Int. J. Rock Mech. Min. Sci. Geomech. Abstr.*, Vol.17, pp.281-288, 1979.

24) Bernabe, Y., Brace, W. F. and Evans, B.: Permeability, porosity and pore geometry of hot-presses calcite. *Mechanics of Materials*, Vol.1, pp.173-183, 1982.

(Received December 20, 1999)